ORIGINAL RESEARCH

The influence of viscose fibre properties on the absorbency of feminine hygiene tampons: the pivotal role of cross-sectional geometry

**T. Harter · A. Wagner · A. Wolfbauer · I. Bernt ·
A. Mautner · M. Kriechbaum · A. Nevosad ·
U. Hirn**

Abstract Feminine hygiene products, used by millions of women worldwide on a daily basis, come in various forms. Among them, tampons are a prominent type that aims to absorb menstrual blood directly in the vagina. However, the underlying mechanisms governing liquid absorption in tampons have received limited research attention and remain poorly understood. This study aims to investigate these mechanisms by examining the two main types of viscose fibres used in tampons and their effects when employed in tampon production. The sole distinction between the fibre types lies in their geometric shape—round or trilobal—while all other fibre parameters remain constant. To explore these mechanisms, tampon proxies made from these fibres were created and subjected to tests measuring liquid absorption. In addition, a novel method employing infrared thermography was utilized to infer the stored energy within the compressed tampon. Furthermore, individual fibres were characterised for chemical composition, surface properties, fine structure, liquid interaction, mechanical parameters, and friction behaviour. The results revealed that trilobal fibres exhibited higher tampon absorbency compared to their round counterparts, despite sharing similar chemical composition and comparable mechanical characteristics. This disparity can be attributed to the greater specific surface area of trilobal fibres, leading to enhanced liquid uptake through fibre swelling. However, single fibre swelling only accounted for a

T. Harter (✉) · A. Wagner · A. Wolfbauer · U. Hirn
Institute of Bioproducts and Paper Technology, Graz
University of Technology, Inffeldgasse 23, 8010 Graz,
Austria
e-mail: harter@tugraz.at

T. Harter · A. Wolfbauer · I. Bernt · U. Hirn
CD Laboratory for Fiber Swelling and Paper Performance,
Inffeldgasse 23, 8010 Graz, Austria

I. Bernt
Kelheim Fibres GmbH, Regensburger Straße 109,
Kelheim, Germany

A. Mautner
Department IFA Tulln, Institute for Environmental
Biotechnology, University of Natural Resources
and Life Sciences Vienna, Konrad-Lorenz-Straße 20,
3430 Tulln an Der Donau, Austria

A. Mautner
Institute for Materials Chemistry and Research, Polymer
and Composite Engineering (PaCE) Group, Faculty
of Chemistry, University of Vienna, Währinger Straße 42,
1090 Vienna, Austria

M. Kriechbaum
Institute of Inorganic Chemistry, Graz University
of Technology, Stremayrgasse 9, 8010 Graz, Austria

A. Nevosad
AC2T Research GmbH, Viktor-Kaplan-Strasse 2/C,
2700 Wiener Neustadt, Austria

minor fraction of the total liquid absorbency of a tampon. The most influential fibre parameter was the geometric shape, as trilobal fibres facilitated the construction and maintenance of a bulkier network with increased available volume for liquid absorption.

products are usually made of cellulosic fibres formed in a nonwoven web, rolled or folded, and pressed into form (Kittelmann 2004; Ajmeri and Ajmeri 2010). Although a relevant product of daily use, tampons are only vaguely described from an engineering point

Graphic abstract
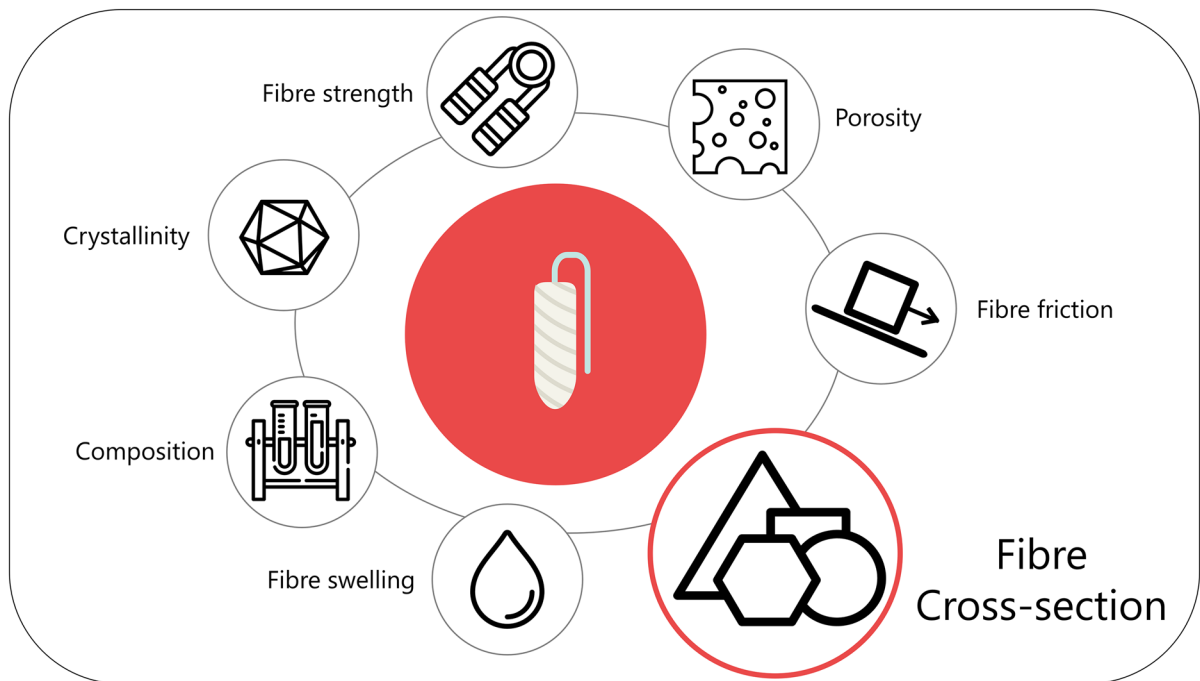
Keywords Tampon · Feminine hygiene · Viscose fibres · Absorbency

Introduction

Tampons are a type of feminine hygiene product designed to effectively absorb large amounts of liquid without leaking, while providing comfort and discretion (Ajmeri and Ajmeri 2010). With a forecasted global market value of 5.43 billion US-Dollar in the year 2023 (Statista 2019) they represent a growing market within the feminine hygiene sector. These

of view, with only few exceptions (Hou and Acton 2016). Most tampons are made using either 100% trilobal viscose fibres or a blend of trilobal viscose fibres and a smaller percentage of standard viscose fibres. The benefits of these fibres comprise their biodegradability (Zambrano et al. 2019), the adjustment of shape and length, as well as the possibility to functionalize them (Fras Zemljic et al. 2011). The cross-section of viscose fibres is defined by the spinning nozzle geometry (Bernt 2011). The shape of tampon fibres is of special interest, as early patents from Procter & Gamble in 1984 (Gellert 1984) and Kimberly–Clark in 1994 (Meirowitz et al. 1994)

mention the use of trilobal fibres in tampons, both of which still produce tampons today. This geometric shape results in much higher absorbency values when used in tampons (Wimmer 2013), compared to standard viscose fibres. The use of super absorbent materials (Ma et al. 2022) has been neglected since the 1980s, when tampons with high absorbency were linked to toxic shock syndrome (Sierks and Reilly 1985; Vostral 2017). Therefore, tampon manufacturers prefer the use of all-cellulose viscose fibres, with trilobal fibres emerging as the top choice. The beneficial properties of trilobal fibres have not been extensively researched, but it is suggested that they depend on their ability to rapidly transport liquid through the channels between the limbs of their unique shape.

Water in cellulose fibre networks

Liquid transportation in cellulosic materials has been thoroughly investigated visually via wicking height (Dubrovski and Brezocnik 2016; Mao et al. 2022), or with more advanced techniques such as cryo-SEM (Senden et al. 2007), confocal laser scanning microscopy (Aslannejad and Hassanizadeh 2017), or infrared thermography (Aslannejad et al. 2017; Murali et al. 2020). IR thermography is a promising and simple technology for studying liquid transportation phenomena, as wetting of cellulose fibres is an exothermic process (Rees 1948). The methods described are utilized to observe liquid transportation, but not to provide a phenomenological description of it.

The Lucas–Washburn equation (Lucas 1918; Washburn 1921) is commonly employed to describe the penetration of liquids into porous materials (Cai et al. 2021), utilizing solid–liquid interfacial parameters to predict the penetration velocity. Trilobal fibres have been shown to have lower advancing contact angles for water and higher surface energies compared to regular round viscose fibres (Whang and Gupta 2000). According to the Lucas–Washburn equation the lower contact angle of trilobal fibres would lead to a higher penetration speed into the substrate. Furthermore, the water uptake of the fibres also affects the wetting dynamics and must be considered when working with hydrophilic materials (Kissa 1981; Kawase et al. 1986). In addition to the Lucas–Washburn equation, a novel approach (Lavi and Marmur 2006; Waldner and Hirn 2023) describes the dynamics of penetration by separately considering the properties of the substrate and the liquid. This alternative approach offers a simpler and more feasible method. In this context, the penetration of the liquid is influenced by the properties of the liquid itself as well as the surface characteristics of the substrate material.

Fibre fine structure and spinning conditions

The transportability of a liquid depends on the fibre structure, as it initially passes through the narrow capillaries on the surface of the fibres (Aslannejad and Hassanizadeh 2017). The lobes and channels of the trilobal fibres were found to facilitate fast liquid transportation, making them particularly advantageous (Whang and Gupta 2000; Gupta 2002), although both trilobal and round viscose fibres come with channels in their geometry (Horio et al. 1947; Nachinkin 1973) which could provide a fast liquid transportation. These channels are created during the production of viscose fibres and are significantly influenced by the spinning conditions, particularly the acidity and the presence of metal sulphates in the spinning bath. The rate of coagulation plays a crucial role in the formation of these channels, with slower coagulation resulting in a higher number of channels in the fibre cross-section. Therefore, a higher acidity in the bath (fast coagulation) (Wilkes 2001) promotes a smoother fibre surface, while an increased amount of added zinc sulphate (slower coagulation) (Klare and Gröbe 1962) leads to a more textured cross-section. Furthermore, the spinning bath, including all the factors mentioned earlier, as well as the draw ratio (which refers to the stretching of the filament), can affect the crystallinity and crystal orientation of the fibres respectively (Wilkes 2001). In summary, the spinning process, in combination with the draw ratio, has a substantial impact on the liquid transportation, liquid uptake properties, and also mechanical characteristics of viscose fibres.

Mechanical considerations on liquid absorption

Liquid uptake also depends on the pore structure of the network that is built and maintained by the fibres within the network (Dubrovski and Brezocnik 2016). Here it is important that the fibres provide enough mechanical stability, even in a swollen

state. As tampons absorb high amounts of liquids for a prolonged time span, the fibres in the tampons start to swell. Water, acting as plasticizer for cellulosic fibres, weakens the fibre strength by breaking up intra-fibre hydrogen bonds (Ganser et al. 2015). The performance of the tampon is greatly affected by the mechanical strength of the fibres in the wet state. Furthermore, fibre–fibre friction can also have an impact on tampon absorbency as it influences the expansion of the tampon by regulating fibre movement (Gupta 2008). Moreover, it contributes to the stability of the wet network by fixing the fibres in place.

Aim of the work

In this work, we will present a comprehensive technological description of the functionality of tampons used for feminine hygiene, which has not yet been undertaken, based on the investigation of the cellulose fibre properties used for their fabrication. Our focus will be on the two primary fibre types used in tampon production: round and trilobal viscose fibres. Trilobal fibres have become the gold standard for tampon production, even though the reasons for their superiority have never been fully defined. Thus, in our study, trilobal fibres are compared to standard viscose fibres that were made using the same spinning dope, in the same spinning bath, and exhibiting the same linear density and length. The fibres were thoroughly investigated and characterised in terms of their mechanical properties, surface characteristics, chemical composition, and their performance when used in tampons.

Materials and methods

Viscose fibres

Cellulose viscose (CV) fibres used in this work enclose two grades. Standard viscose fibres with a round, irregular cross-section and trilobal viscose fibres. Both fibre grades have a linear density of 3.3 dtex and a fibre length of 40 mm. The fibres were produced from the same batch, using the same viscose dope and spinning conditions and were provided by Kelheim Fibres GmbH.

Tampon proxy production

Tampon proxies were produced by Kelheim Fibres GmbH, using approximately 100 g of cut fibres to manufacture a carded dry-laid web. The web was conditioned at 20 °C and 65% RH, and several layers of cut sheets were then placed on top of each other until a mass of 2.7 g was achieved. The sheets were folded and pressed into small cylinders with a diameter of 13.90 ± 0.16 mm and a height of 30.81 ± 0.17 mm. The resulting plugs were then placed inside polycarbonate husks and stabilized using microwaves at 900–1100 W for 45 s. The final fibre packing density in the tampons was consistent between both types of fibres, at approximately 0.4 g/cm^3.

Tampon absorbency

The performance parameter of tampons is their liquid absorbency, measured with a syngina (synthetic vagina) setup, following the industrial standard procedure (Reame 2020). The main aspect of this setup is a controlled environment where the tested tampon expands during a defined liquid application. Therefore, the sample is placed inside a membrane that is mounted to a glass device, as shown in Fig. 1.

Fig. 1 Syngina setup with tested sample in the middle, liquid supply from the top and 27 °C deionized water surrounding the sample

Fig. 2 Microtome cuts of exemplary round and trilobal fibres used in this work. The typical crenelated structure of viscose fibres can be seen in the round fibre
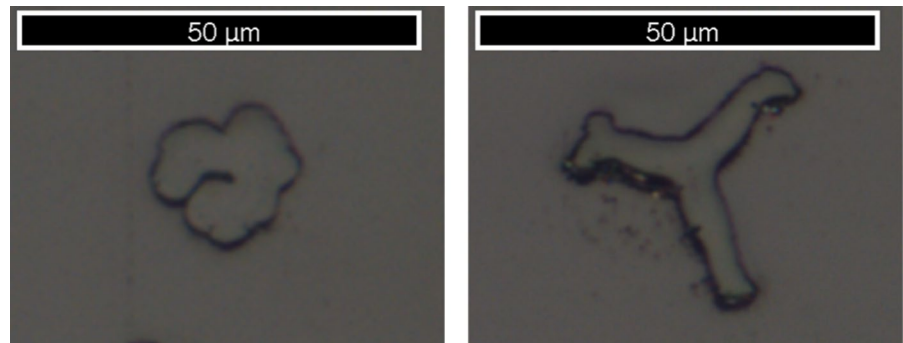
The glass device is necessary to immerse the tampon inside the membrane in water, which is maintained at a temperature of 27 °C. The hydrostatic pressure inside the glass device is set to a moderate pressure of 1773 Pa and the device is tilted by 30° from vertical axis. Inside the membrane a syringe pump applies the testing liquid on top of the tampon at a constant rate of 50 mL/h. The standard testing liquid consists of 1 L deionized water, 10 g NaCl and 0.5 g Allura red dye. The test is considered complete once the liquid exits the bottom of the tampon. The sample is weighed before (m_{before}) and directly after the test (m_{after}) and the specific syngina absorption is calculated using Eq. (1).

$$Specific\ syngnia\ absorption \left[\frac{g}{g}\right] = \frac{m_{after} - m_{before}}{m_{before}} \tag{1}$$

Fibre swelling (WRV)

The swelling capacity of the fibres was determined by applying pulp standards (ISO 23714). Therefore, the fibres were immersed in deionized water at a concentration of 5 g/L for at least 4 h after which the fibre were dewatered, using a Büchner funnel. The dewatered pads were then centrifugated with a laboratory centrifuge (SIGMA 3–15) at a relative centrifugal force of 3000 g for 30 min. The sample was then weighed (m_{cent}), dried overnight at 105 °C, and weighed again (m_{OD}). The water retention value was calculated using Eq. (2).

$$WRV \left[\frac{g}{g}\right] = \frac{m_{cent}}{m_{OD}} - 1 \tag{2}$$
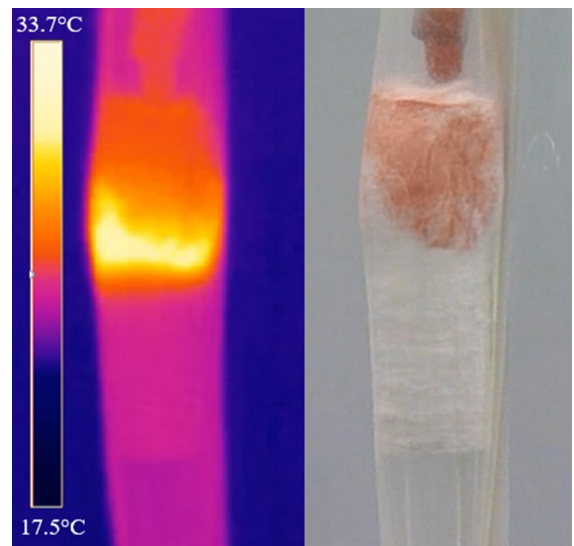

Fig. 3 Infrared image and CMOS image of a tampon proxy at the same time. The front of the IR is ahead of the optical visible liquid front

Mechanical properties

Measurements of the mechanical characteristics of the fibres were carried out using a TA Instruments Discovery DMA 850. Tensile tests were performed at varying relative humidity. Single fibres were directly mount to the clamps of the DMA machine before the relative humidity was adjusted at a rate of 2 RH/min. After the defined relative humidity was reached, a soaking time of 30 min was initiated. The temperature for all measurements was set to 23 °C. Tensile testing was performed at a rate of 6 mm/min for a duration of 6 min to ensure that the breaking point was reached. Stress calculation was done using the cross section of the fibres at 50% RH, obtained via microtome cuts

Fig. 4 Filament on carrier bodies, after a dry experiment

(cf. Fig. 2). For the wet samples 1.5 times the dry cross-section was used, as literature suggests that cross-section increase due to swelling for viscose fibres is about 50% (Preston and Nimkar 1949). The Young's modulus was calculated from the obtained stress–strain curves using MATLAB. The stress data, which was highly scattered, was smoothed using a Gaussian smoothing function. The highly scattered stress data was smoothed using a Gaussian smoothing function. Then, for each position on the stress–strain curve, the Young's Modulus was obtained by calculating the tangent using ten data points and moving the curve to align the corresponding linear portion with the origin of the coordinate system. Subsequently, the strain at which the material breaks was determined. Using the tangent at the maximum strain, the Young's Modulus was calculated. This procedure allowed us to calculate the Young's modulus even for stress–strain–curves where an irregular drop in the strain data occurred in the elastic region. This method correlates well with standard calculations, such as obtaining the maximum slope in the elastic region.

Infra-red thermography

Heat development in tampons during liquid application was observed by thermography using a long wavelength infrared camera (LWIR, Optris PI450). The sample tampon was therefore mounted to a wooden frame inside a membrane. The same liquid as in the absorbency tests was applied on the top of the sample at the same rate of 50 mL/h representing

the first measurement. During that measurement the IR camera collected the temperature data every 10 s in a spreadsheet until 100 datasets were generated. Figure 3 illustrates a comparison between an infrared image and an optical image (CMOS) of a tampon proxy taken simultaneously. The leading edge of the heat observed through IR is situated farther away compared to the visible liquid front observed optically. The sample was then centrifuged (30 min at 3000 g) and airdried at 23 °C and 50%RH for one week, before tested again (second measurement). For a third measurement, this procedure was repeated on more time for each sample. Evaluation of the data was done by generating mean curves for the maximum observed temperature of 5 samples each for the first, second and third measurement, using MATLAB.

X-ray photoelectron spectroscopy (XPS)

X-ray photoelectron spectroscopy (XPS, Nexsa, Thermofisher) was used to study the surface composition of the cellulose fibres using Al Kα radiation at 72 W. A pass energy of 200 eV, a spot size of 400 μm, "Standard Lens Mode", CAE Analyser Mode, and integrated flood gun were used at an energy step size of 1 eV for the survey spectrum (50 passes), Samples were analysed prior to and after the surface was treated with Ar-clusters (1000 Ar atoms, 6000 eV) for various time intervals. High-resolution spectra of the single elements were recorded at a step size of 0.1 eV with 50 passes at a pass energy of 50 eV. Data evaluation was performed with Thermo Avantage v5.9925 Build 06702 using "Smart" background.

Inverse gas chromatography (iGC)

n-Octane adsorption isotherms were evaluated using iGC (iGC-SEA, Surface Measurement Systems Ltd., Alperton, UK). Approximately 450 mg of the various types of viscose fibres were packed into a glass column with an internal and external diameter of 4 mm and 6 mm, respectively. Prior to the measurement, the sample was conditioned at 30 °C for 1 h to remove. *n*-Octane was then injected at different relative pressures (p/p0) at 30 °C. The retention volumes of *n*-octane at various p/p0 were determined by analysis of the peak maximum (PM) or centre of mass (CoM). Methane was used to determine the dead time of the packed column.

Fig. 5 Open sample holder with mounted bundles of fibre (left) and closed with the fibres fixed between two metal plates (right)
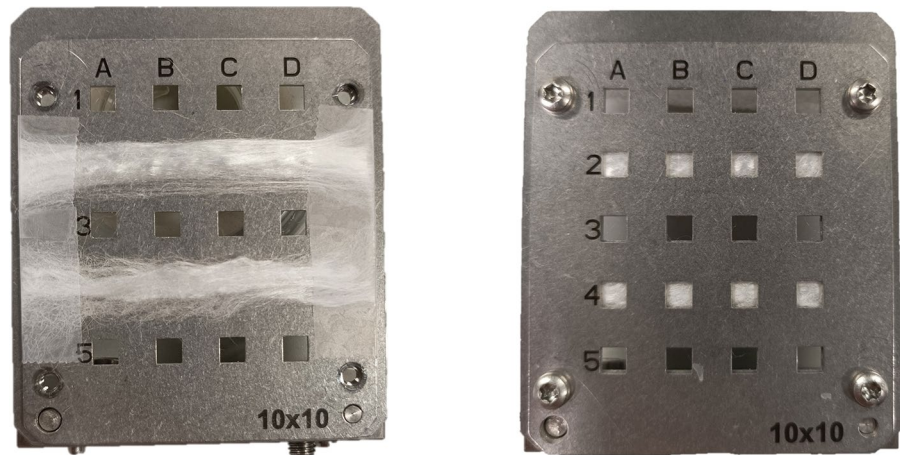
Friction measurement

In order to measure the coefficient of friction between fibres of the same kind in dry and wet conditions, filament was wrapped on 2 aluminium carrier bodies, one being a cylinder with a diameter of 8 mm the other one a flat cuboid, as displayed in Fig. 4. These specimens were mounted in a Universal Mechanical Tester (UMT) from Tribolab for the tribological measurements. The machine was set to an oscillating movement, driven by a crank mechanism with a stroke of 5 mm at a frequency of 2 Hz and the first 10 full cycles were used for the data evaluation. As normal force 5 N were chosen. The resulting pressure cannot be stated due to the soft and flexible nature

of the fibres which does not allow a determination of the contact area. Every set was repeated 3 times, each with new filaments. For the wet experiments, the specimens were immersed in deionized water prior to the testing.

Crystallinity: wide-angle X-ray scattering (WAXS)

Bundles of the fibre samples were mounted oriented horizontally on a motorized X/Y-stage, as depicted in Fig. 5. Wide-angle X-ray scattering (WAXS) measurements were carried out with a laboratory S(W)AXS instrument (SAXSpoint 2.0, Anton Paar, Austria) using point-focused/slit-collimated Cu-Kα radiation with a wavelength of 0.154 nm from a micro-source operating at 50 W and equipped with a
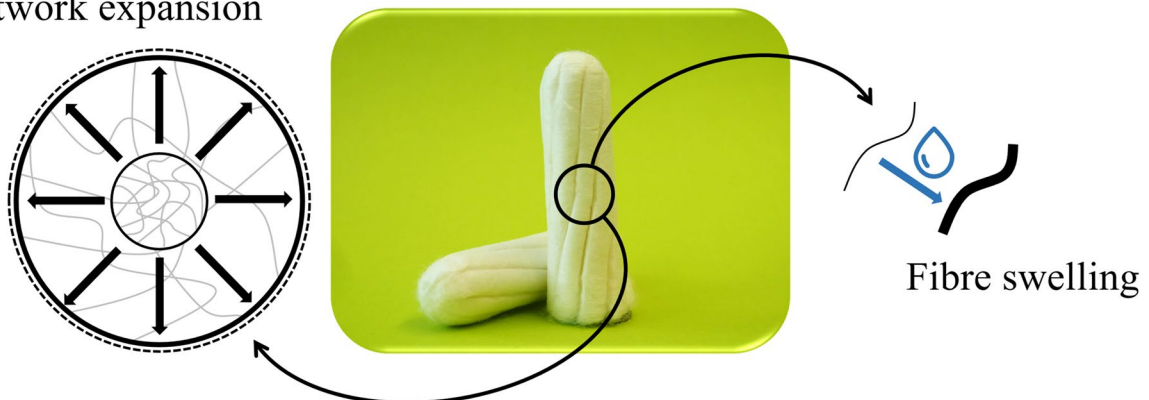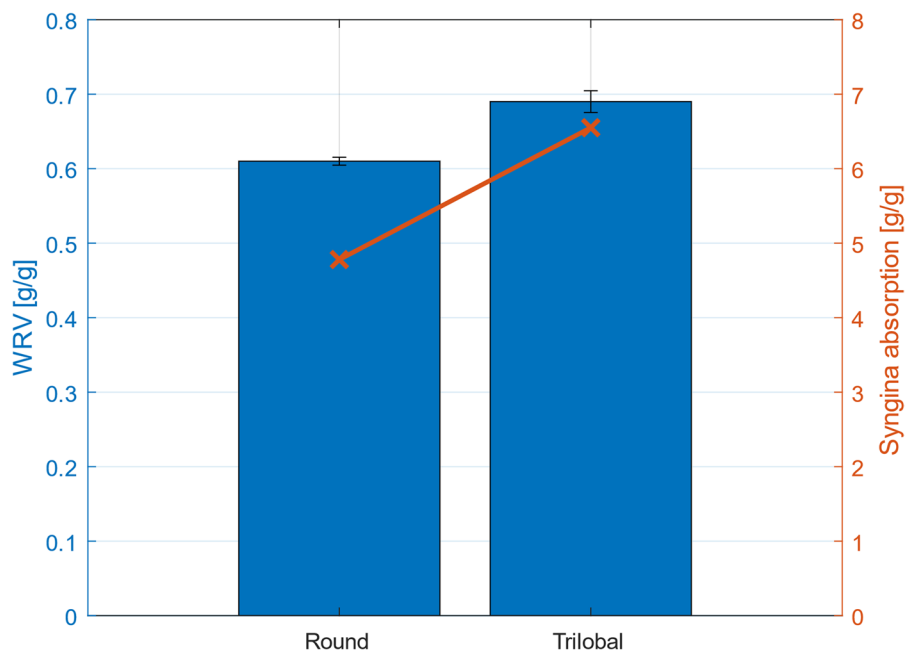

Fig. 6 Two mechanisms that are relevant for liquid absorption of feminine hygiene tampons

Dectris EIGER2 R 1 M hybrid pixel area X-ray detector (Dectris, Baden-Daettwil, Switzerland).

2D WAXS patterns of the samples were recorded in vacuum (~ 1 mbar and 25 °C) by choosing a sample-to-detector distance of 150 mm. Exposure times were usually 30 min. All 2D-WAXS patterns were azimuthally integrated (opening angle 45 °C) in order to obtain the 1D-WAXS curves with the scattered intensities as a function of the scattering angle in direction parallel or perpendicular to the fibre axis. The calculation of the crystallinity index was performed using a peak deconvolution method proposed elsewhere (Hindeleh and Johnson 1974; Sun et al. 2015).While peak deconvolution is only utilized in 5–10% of studies investigating the crystallinity index of cellulose materials, it is the preferred method for regenerated fibres (Park et al. 2010). Therefore, a 3rd order polynomial was fitted as the amorphous halo to the normalized WAXS signal. The difference between original signal and the amorphous part was fitted with 10 gaussian curves and the crystallinity was calculated using Eq. (3).

$$Crystallinity[\%] = \frac{Area under crystalline part of the signal}{Area under original signal} \times 100 \quad (3)$$

Results and discussion

Mechanisms in tampon absorption

Tampon absorption is a complex and dynamic process. The liquid is absorbed by the fibres and the inter-fibre pore system, and transported throughout the network, resulting in the expansion of the tampon and the creation of additional pores for further liquid uptake. Figure 6 illustrates that tampon absorption is driven by two factors: fibre swelling and network expansion. After 15–20 min under standardized conditions, the absorption process of the tampons used in this study ends and leakage occurs. The elasticity of the fibres plays a critical role in the expansion of the network, particularly since the nonwoven fabric undergoes significant compression during tampon production. This compression can either cause plastic deformation of the fibres or keep elastically deformed fibres in a constrained state. When a liquid is applied to the tampon, it can relieve the compression on the fibres, enabling them to expand and create a porous network with larger pores that can absorb and retain liquid. Moreover, the stored energy in the system is a crucial driving factor for expansion. Figure 6 illustrates that in addition to network expansion, fibre swelling is also a key factor in tampon

Fig. 7 Syngina absorption (orange) and water retention values (blue) for tampon proxies made of 100% round viscose fibres and 100% trilobal viscose fibres

Fig. 8 Comparison of the total tampon absorption and fibre swelling. The basis for these calculations is the overall absorption of the respective fibre type
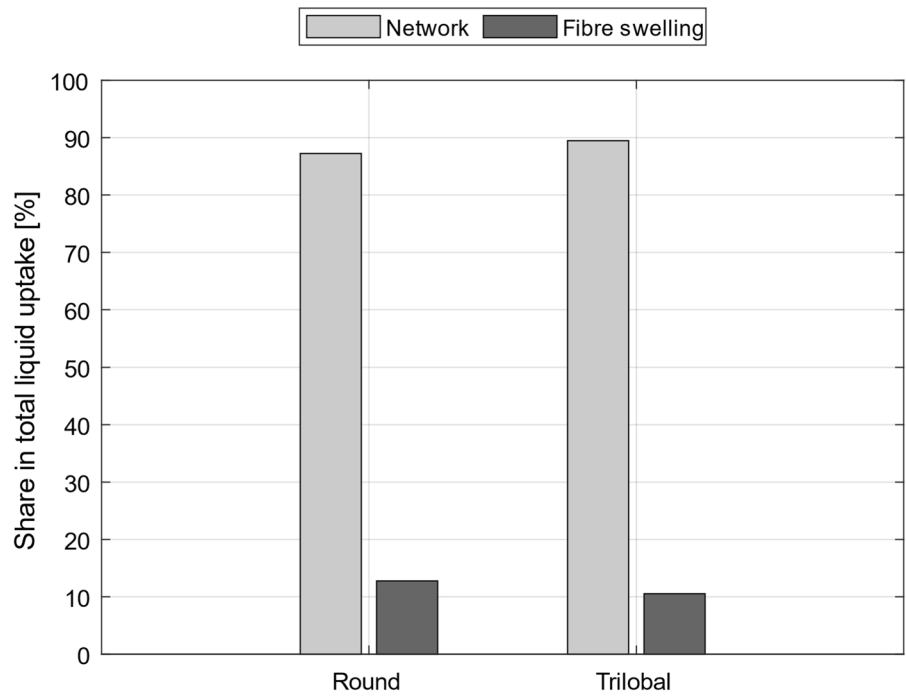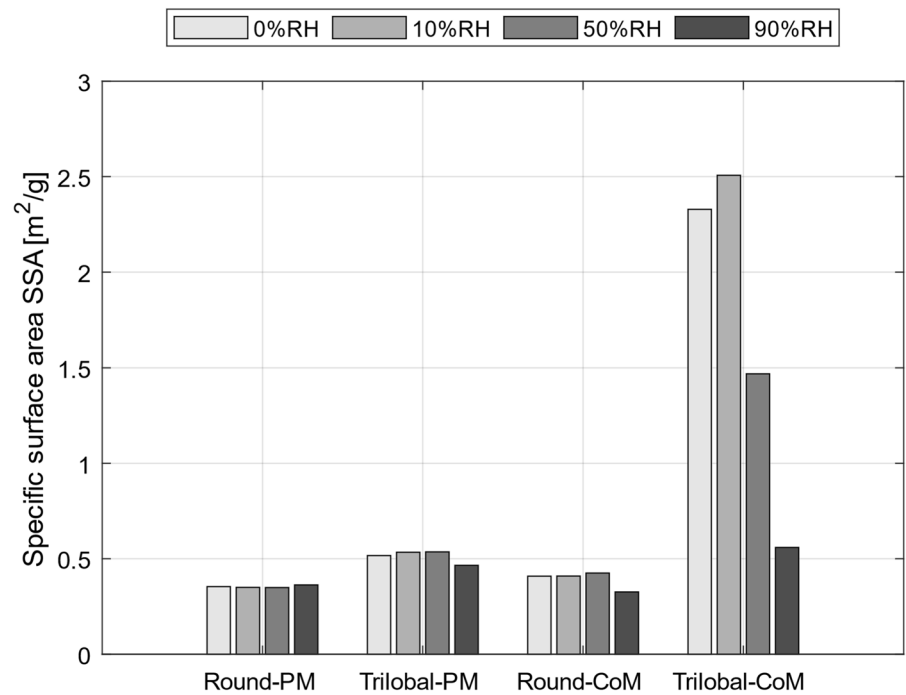

Fig. 9 Specific surface area via IGC measurement—Two types of BET evaluation: peak maximum (PM) and centre of mass (CoM)

absorption. The specific surface area is of particular interest for fibre swelling, as they enable the fibre to absorb more water.

Syngina-absorption and fibre swelling

Figure 7 displays the liquid absorption (syngina absorption), representing tampon performance, and the swelling capacity or water retention values (WRV) for tampon proxies made exclusively from round fibres, respectively trilobal fibres. Despite being produced from the same spinning dope and coagulated in the same spinning bath, trilobal fibres offer higher liquid absorbency as well as higher swelling capacity when used in tampons.

While the increased swelling of trilobal fibres may explain their greater tampon absorption capacity, Fig. 8 contradicts this explanation to some extent. Here, the fibre swelling (WRV) was compared to the liquid absorbency of the tampons (syngina). It was observed that fibre swelling accounts a mere 13% of the total liquid absorption in round fibres and 11% in trilobal fibres in tampons. Despite having higher water retention values, the share of liquid absorption in trilobal fibres is slightly lower compared to round fibres, due to the higher overall absorption found in

trilobal fibre tampons. However, for both fibres, the contribution of fibre swelling to tampon absorption is relatively low. Thus, fibre swelling does contribute to the overall liquid absorption but is not the predominant factor. Nevertheless, fibre swelling can enhance tampon performance to some extent.

Specific surface area of the viscose fibres

Even though fibre swelling plays a minor role in liquid absorption, it is still intriguing to understand how fibres with the same linear density, produced under identical conditions from the same precursor material, exhibit varying water uptake. To gain insights into the water uptake mechanisms of these two fibre types, their specific surface area (SSA) was examined (Fig. 9). The specific surface area of the two fibre types was calculated using BET theory by measuring the retention time of octane at varying p/p0 and relative humidity. Two different methods were employed for the evaluation of the obtained chromatography data, peak maximum (PM) and centre of mass (CoM). The primary results indicate that trilobal fibres generally exhibit higher SSA than round fibres for both PM and CoM, in particular at a relative humidity of 0%, 10%, and 50%, respectively, which

Fig. 10 Results of the XPS measurements showing the ratio of C1*s* to O1*s* of the fibre types. Error bars represent one standard deviation
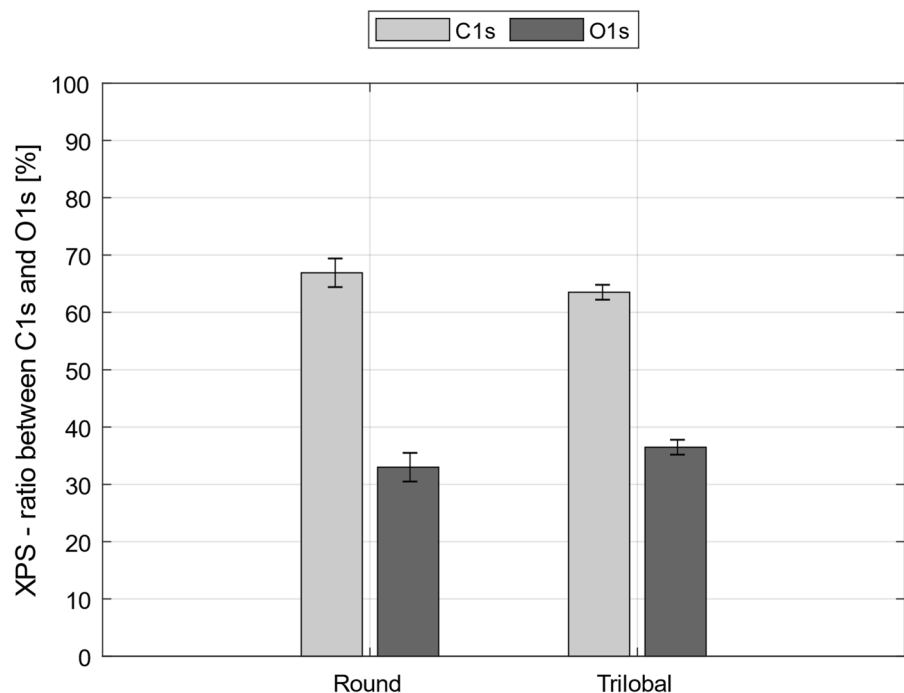
Fig. 11 WAXS diffraction patterns (2D) and intensity signal over 2Θ (1D) for round CV. The evaluation of the signal is depicted as the 3rd order polynomial amorphous halo and the Gaussian fit to the crystalline signal
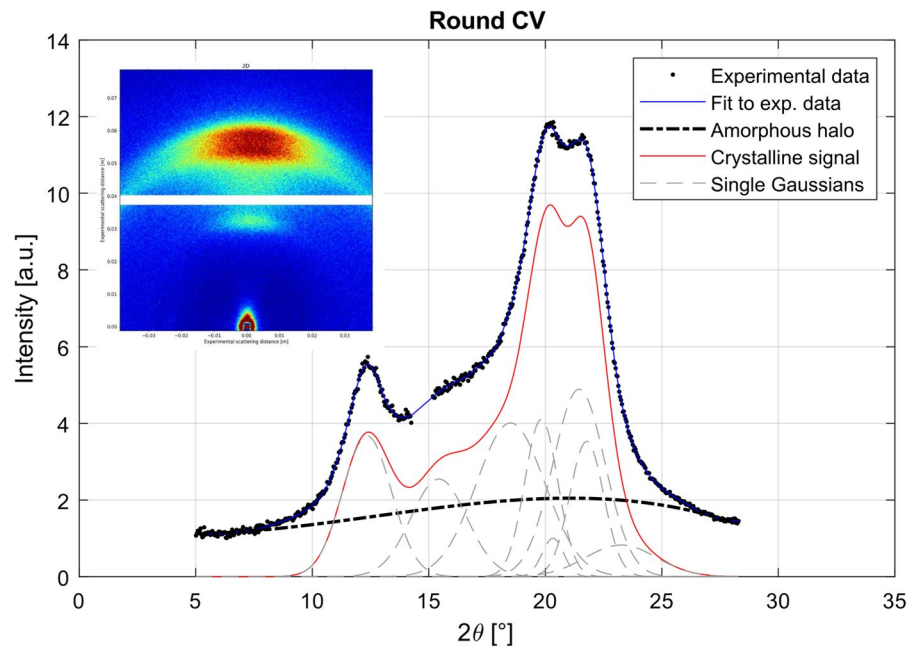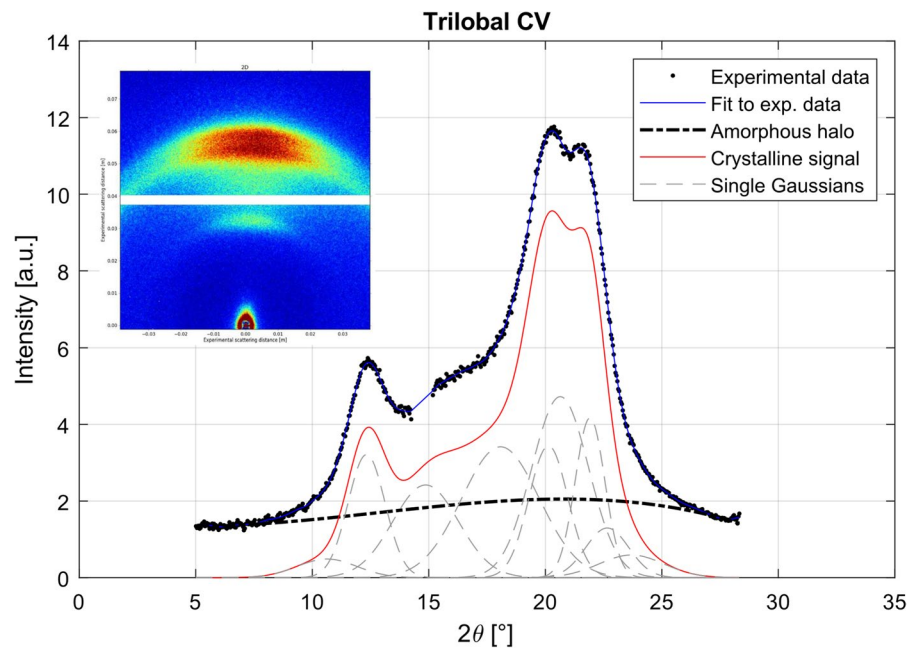

Fig. 12 WAXS diffraction patterns (2D) and intensity signal over 2theta (1D) for trilobal CV. The evaluation of the signal is depicted as the 3rd order polynomial amorphous halo and the Gaussian fit to the crystalline signal

is in good agreement with the higher water retention values observed for the trilobal fibres. However, at high relative humidity (90%), the fine pores of the fibre may already be occupied by water molecules, thereby limiting the access of the pores to the octane used in the iGC measurement. Viscose fibres usually come with very small pores in the nanometre

range (Krässig 1993), which are also indicated by the higher SSA values when using CoM for data evaluation. Higher values obtained from the CoM evaluation are a hallmark for deep, narrow pores that can retain the mobile phase in the iGC (e.g. octane) for a longer time (Conder and Young 1979). The higher SSA of the trilobal fibres most likely originates in

their geometric shape, as both fibres are made of the same precursor material. Also, the coagulation bath, which is known to be to be a potential influence of the porous structure (Krässig 1993; Nikonovich et al. 2007), was the same for both fibre types. It seems, however, that the trilobal geometry under comparable spinning conditions provides both a higher specific surface area and enhanced water retention.

Elemental surface composition by XPS

The fibres investigated in this study were produced using the same spinning dope and coagulated in the same spinning bath with the same draw. Therefore, the chemical composition of both fibre types should be similar. Figure 6 shows the mean values of five of the XPS measurements on one sample taken at different positions after 150 s of Argon cleansing representing the surface elemental composition of the fibres. No significant differences between the two fibre types were observed, indicating a certain chemical similarity between the two samples (Fig. 10).

Crystallinity index by WAXS

Crystallinity describes the amount of well-ordered regions in a polymer and can be linked to several parameters. Higher crystallinity in cellulose increases strength and decreases elasticity, swelling and suitability for chemical reactions (Luan et al. 2022). Utilization of WAXS for crystallinity measurements in cellulose fibres is commonly used and well described (Park et al. 2010; Sun et al. 2015). Although different evaluation methods (e.g., peak deconvolution) can yield different crystallinity values (Ahvenainen et al. 2016), it can be a useful method to compare samples were measurements and evaluation are done in the same way. Figures 11 and 12 depict the results of WAXS measurements and evaluation for round and trilobal viscose fibres. There the intensity is drawn over the scattering angle 2Θ and inserts show the original 2D diffraction patterns. Both fibre types provide a similar WAXS signal and the evaluation exhibits similar crystallinity values of 62.95% ± 1.81% for round CV and 60.62% ± 2.50% for trilobal fibres.

The difference between the round CV and trilobal CV are rather small and indicate an elevated amount of well-ordered regions for round fibres. More amorphous sites on fibres are connected to a higher water

Fig. 13 Ultimate tensile strength of single fibres at varying relative humidity. 100% relative humidity represents wet samples that were soaked in water for several hours
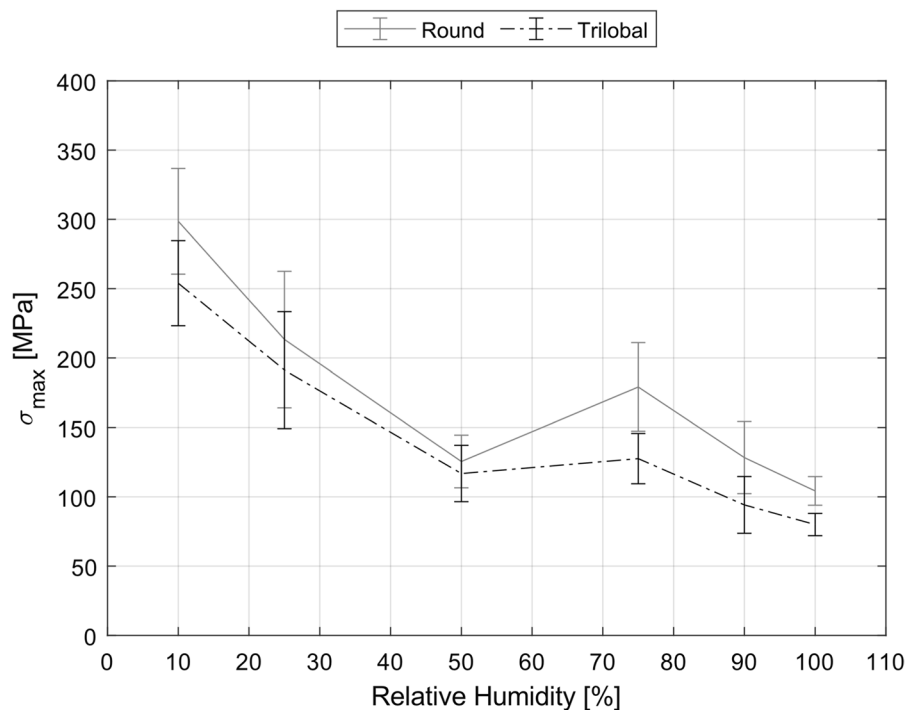
Fig. 14 Young's modulus of viscose fibres at different relative humidity. 100%RH represents wet samples that were soaked in water for several hours
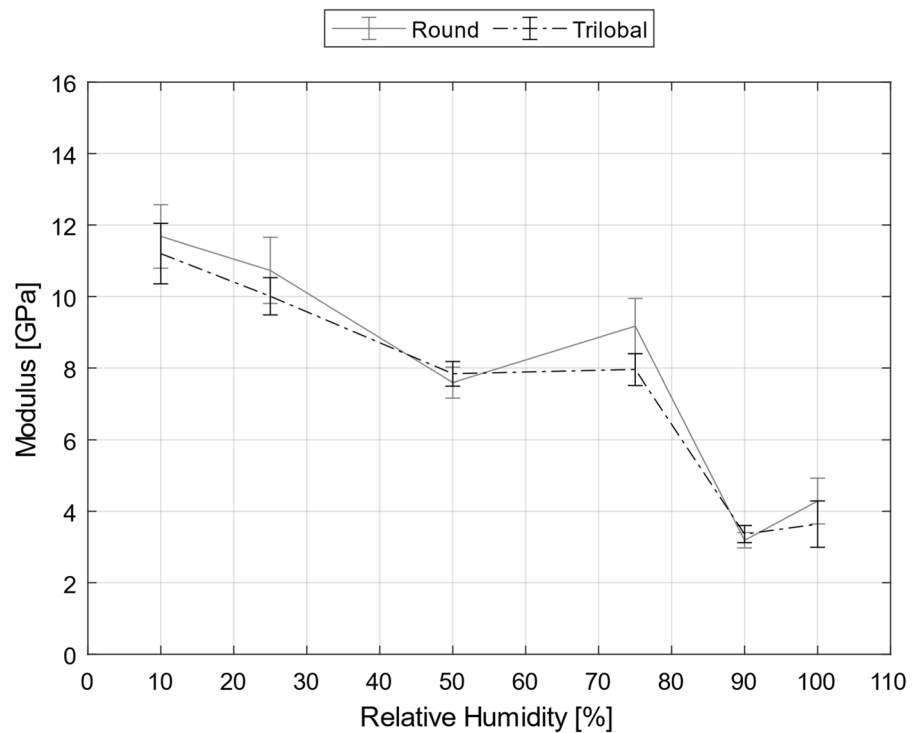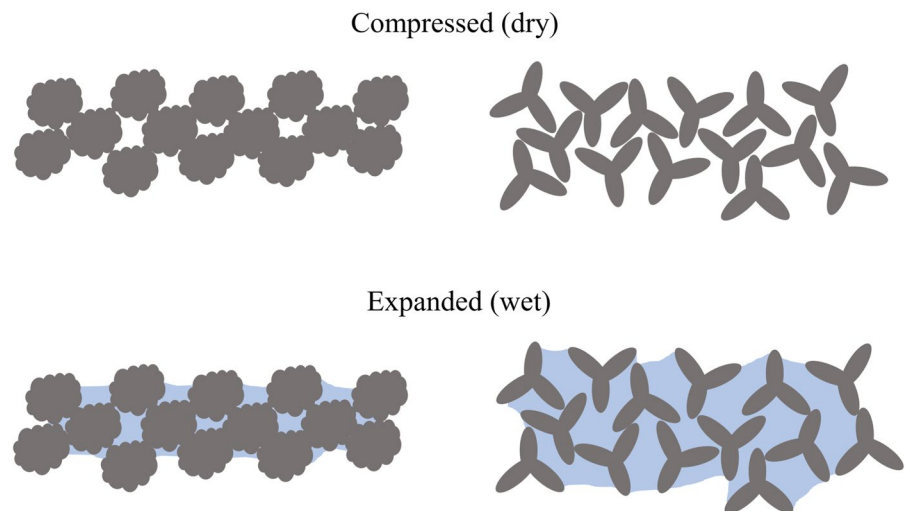

Fig. 15 Top: Compressed fibres in a tampon made of round fibres (left) and trilobal fibres (right). Bottom: Schematic liquid distribution in an expanded network of the same fibres

Compressed (dry)

Expanded (wet)

uptake and WRV is higher for the tested trilobal fibres (cf. Fig. 7). In other publications it was described that water uptake of regenerated fibres is connected to the specific surface area and not the fibre crystallinity (Kreze and Malej 2003). This also correlates well to our findings in the iGC measurements, as shown in Fig. 9. However, the crystallinity differences are rather small and indicate that the cross-section has

only a minor influence on the crystallinity, as long as spinning dope, coagulation bath and the draws are kept constant during production.

Single fibre strength and elastic modulus

From investigating the chemical composition of round viscose fibres and trilobal fibres through XPS

respectively, no significant difference was found to explain the superior tampon performance of trilobal fibres, suggesting that the cause may lie in their geometry. Moreover, the mechanical properties of the fibres could be critical since the network must be strong enough to retain a porous and bulky structure when liquid is applied. Hence, it appears essential to examine the strength properties of both fibre types.

Figure 8 clearly shows that tampon absorption is predominantly a network property and therefore depending on the structuring elements, i.e., the fibres. It seems therefore advisable to take a closer look onto single fibre mechanics. Figure 13 depicts the ultimate tensile strength of single viscose fibres at different levels of relative humidity. After 50% RH, the mechanical strength of the fibres generally decreases as humidity increases, with the lowest strength observed for fibres soaked in water (100% RH).

Both fibre types show similar strength, with slightly higher values obtained for the round fibres, which may be connected to the higher crystallinity in this fibre type. The strength of the wet samples (100%RH) shows only small differences with 104 ± 10 MPa for the round fibres, compared to 80 ± 8 MPa for the trilobal fibres. It is surprising that the two fibre types exhibit similar strength when wet,

given that the trilobal fibres absorb approximately 15% more water, which typically acts as a plasticizer on cellulose-based materials (Ganser et al. 2015). Although the tensile strength is also slightly lower for wet trilobal fibres, the Young's modulus is the same for both fibre types at different relative humidity, as shown in Fig. 14. The values for the wet samples are almost identical, despite the fact that trilobal fibres absorb more liquid. This is especially interesting as a plasticizer should influence the stiffness of the materials, but the Young's modulus is the same for both fibre types.

The data in Figs. 13 and 14 demonstrates that there are no relevant differences in mechanical parameters between the round and trilobal fibres. Both fibre types exhibit a similar decline in strength and modulus with increasing relative humidity. Differences in mechanical properties does therefore not seem to explain the superior tampon performance of trilobal fibres. Other testing modes, e.g., bending (Gupta 2002), could help to gain better understanding the load condition during liquid absorption of tampons. It is possible that strength of the single fibres may not be the dominant parameter in tampon absorption, and that both fibre types could provide a stable network. However, due to geometrical reasons, trilobal fibres may provide more

Fig. 16 Coefficient of friction for both fibre types in the dry and the wet state
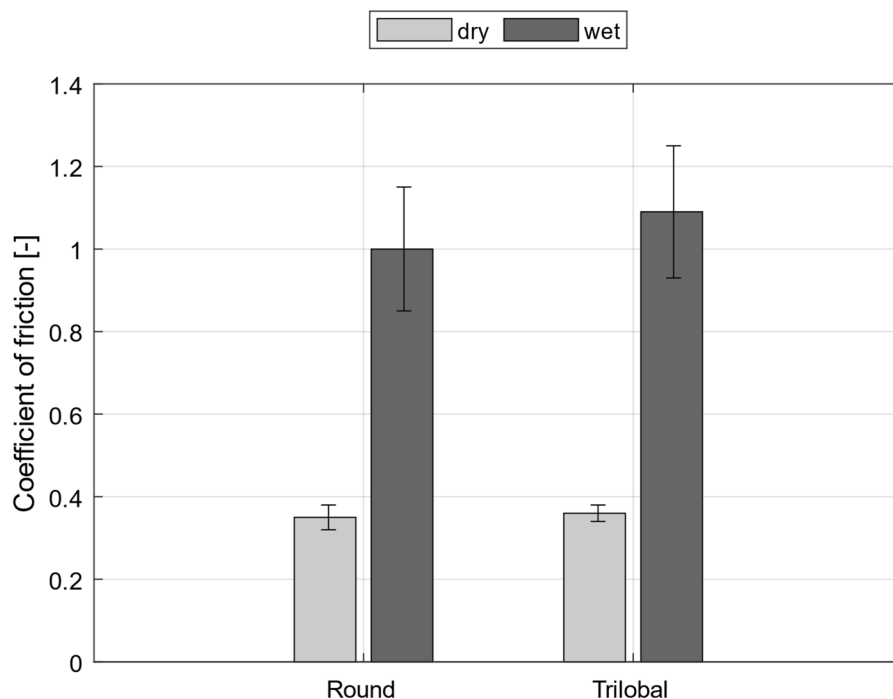
or larger pores (Fig. 15). Here, trilobal fibres create and maintain a more open structure during liquid application, consequently providing higher porosity. The densities of the expanded tampons further confirm this observation, as tampon density and porosity share an inversely related relationship. Tampon proxies made of round viscose fibres expand to a density of 0.129 ± 0.007 g/cm^3 (lower porosity), whereas expanded trilobal fibre tampons exhibit a lower density of 0.093 ± 0.002 g/cm^3 (higher porosity). The absolute fibre mass was the same in all tested tampons. Therefore, trilobal fibres create a larger volume during expansion with a higher pore volume for liquid uptake, as shown in Fig. 15. This could be due to the shape of the fibre, which can be easily compressed (Kara et al. 2012) during tampon production. Both fibre types demonstrate a secure fit in the compressed state. While this characteristic is understandable for round cross-sections, it is noteworthy that trilobal fibres are also capable of forming a compact structure under the applied pressure during tampon production. In this case, the lobes of the trilobal fibres are able to effectively occupy the available open space. However, in the expanded state, trilobal fibres exhibit the ability to form an open and porous structure that can accommodate a larger volume of liquid compared to round fibres. It is also possible that the narrow channels

formed by the trilobal fibres may lead to higher capillary pressure, which, in turn, might drive the liquid to permeate deeper into the core structure of the tampon, consequently increasing its overall absorbency. Because the unexpanded tampons made from both fibre types exhibit similar density, they possess comparable initial porosity. As a result, when liquid is applied, capillary pressure is on a similar level in both types of tampons. However, capillary penetration in porous substrates is dependent on more parameters such a pore shape, tortuosity and the pore wall structure (Waldner and Hirn 2023).

Nevertheless, it remains a possibility that trilobal fibres have a faster porosity-increasing capability following liquid application. This potential difference could stem from factors like the storage of higher elastic energy in these fibres during tampon production, in contrast to round fibres. Additionally, distinctions in the inter-fibre movement during expansion might contribute to this phenomenon.

Fibre–fibre friction as a network expansion parameter

While the mechanical strength of tampon fibres describes their ability to build and maintain a porous network structure, the friction between the fibres is an important parameter in network expansion. In the dry

Fig. 17 Temperature increase during liquid application for round fibre tampon proxy measured by infrared thermography. Dense lines represent average curves of 5 measurements. Tampon proxies were tested three times consecutively
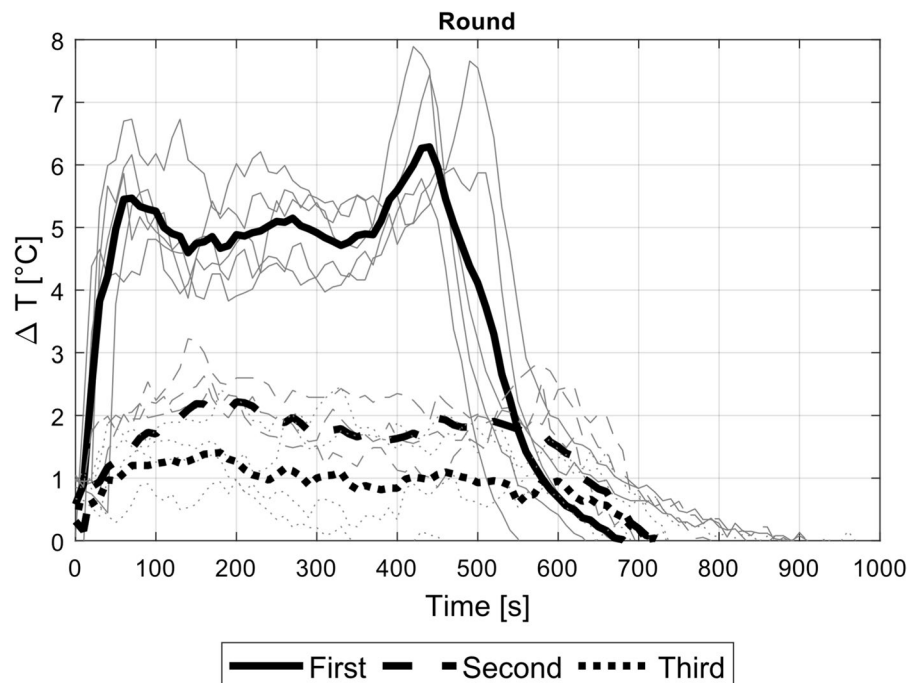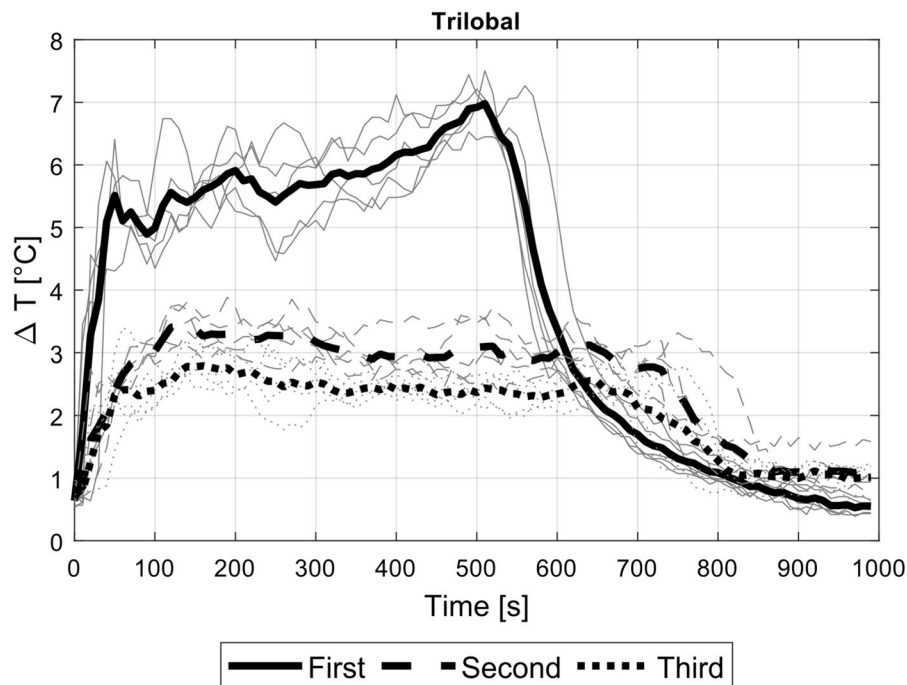
Fig. 18 Temperature increase during liquid application for trilobal fibre tampon proxy measured by infrared thermography. Dense lines represent average curves of 5 measurements. Tampon proxies were tested three times consecutively

state, fibre–fibre friction is relevant for the stability of the compressed tampon, while the coefficient of friction in the wet state is important for expansion, i.e., the ability of the network to expand and build a bulky structure. Figure 16 shows the coefficient of friction for both types of fibres in dry and wet conditions. The displayed coefficient of friction corresponds to the measured maximum values of the cyclic friction experiments. These maximum values were measured not at the turning points of the oscillating movement, as would be expected for a conventional material pairing with a transition from static to dynamic friction, but at a significant relative movement of the specimen. This is due to the soft and flexible nature of the material, which allows significant displacement of the fibres prior to sliding and therefore a defined transition from static to dynamic friction cannot be identified. Neither the dry fibres nor the wet fibres exhibit any differences in friction behaviour between the fibre types. Round and trilobal fibres, therefore, have similar premise for expansion. The higher values for wet fibres could be a result of capillary bridges formed between the fibres during the measurement, resulting in increased adhesion and therefore higher coefficients of friction compared to dry samples. Another explanation could be that due to the lower

elastic modulus of the wet fibres, the contact area is increased and the softer fibres show a higher tendency for interlocking, which therefore further increases the apparent coefficient of friction.

Liquid movement and stored mechanical energy by IR thermography

For the full picture of parameters influencing tampon absorbency, further properties such as the ability of the network to expand, are to be investigated. For that, stored mechanical energy in the network, i.e., tampon, would be a relevant parameter.

Infrared thermography has been used before to observe liquid movement in cellulose networks (Aslannejad et al. 2017; Murali et al. 2020). The heat of sorption released during the exothermic interaction between the solid phase (fibre) and the liquid phase (water) allows the tracking of a liquid in a cellulose network. Typically, the heat of sorption is determined via mathematical models and measurements of the water content of a cellulosic sample under varying relative humidity and constant temperature (isothermal), or through reaction calorimetry (Leuk et al. 2016). IR thermography is also capable of detecting regions of failure in the cellulose network (Lahti et al. 2020), although in this case, the measurement

captures the irreversible energy release resulting from the breaking of fibre bonds.

Figures 17 and 18 depict the temperature development in tampons during liquid application. The temperature difference ΔT describes the temperature increase in the tested tampons, as a consequence of a liquid that is applied on the tampon at constant rate. It is defined as the difference between the maximum observed temperature at each time step and the temperature before the liquid application started (i.e., room temperature). The test is conducted on the same sample three times consecutively, with airdrying at 23 °C and 50% RH for at least 72 h between each test. During the first test the tampon expands and the largest temperature increase is observed. During the second and third test minor differences can be seen and the tampon exhibits no significant expansion anymore.

During the first measurement, the maximum temperature increase for tampon proxies made of trilobal fibres was 7.0 °C, which is higher than the 6.3 °C for those made of round fibres. These values were obtained from the dense average curves in Figs. 17 and 18. The grey lines, representing the single measurements, indicate that these differences are not significant. However, ΔT for the second and third measurements are significantly higher for trilobal fibres, indicating stronger solid–liquid interactions, i.e., heat of sorption, in these tampons. This is consistent with the observations in the iGC measurements, where trilobal fibres were shown to have a higher SSA, providing more sites for solid–liquid interactions.

The high ΔT for the first measurements are indeed remarkable. Although it was previously reported that temperature increases during wetting, so far it has only been reported that this temperature increase is limited to 3 °C for cellulosic materials (Murali et al. 2020). A change in emissivity of the materials due to swelling of the fibres can be neglected, as demonstrated elsewhere, that the emissivity of dry and wet cellulosic fibres is similar and somewhere around 0.9 (Aslannejad et al. 2017). In addition, the emissivity would only increase during water swelling, as the uptake of water would result in an emissivity that is closer to that of water (Hyll 2016). If the emitted radiation energy is kept constant, a higher emissivity would result in a higher observed temperature, according to the Stefan–Boltzmann law. Therefore, an increasing

emissivity would only dampen our results, and we would obtain even higher temperatures.

The tampons expand during the first test, resulting in a higher temperature compared to the second and third tests. The significantly higher temperature in the first test may be due to the mechanical energy stored in the tampon during production, specifically the press-forming of the tampons. This energy may be the driving force behind tampon expansion during liquid absorption. Although there is only a small difference in the first measurement of trilobal fibre tampons and round ones, it still supports the idea of released stored energy. Here, a slightly higher energy can be observed for trilobal fibres, as described elsewhere (Roggenstein 2011). While both fibre types have the same expansion potential, only trilobal fibres can maintain an open structure, while the network of round fibres collapses due to their shape. However, fibre geometry still seems to have the highest impact on tampon performance.

Conclusions

In this study, the performance of two commonly used tampon viscose fibre types, round standard fibre and trilobal fibre, were compared. Tampons made of trilobal fibres have higher absorption capacity than those made of round fibres, with higher water retention values for trilobal fibres. This could be attributed to the higher specific surface area of trilobal fibres. However, fibre swelling alone cannot fully account for the higher tampon absorption as it only contributes to around 11–13% of the total liquid uptake of tampons. The ultimate tensile strength and Young's modulus of both fibre types are similar over a wide range of relative humidity, even when the fibres are completely saturated with water. This is noteworthy because the trilobal fibres swell 15% more than round fibres, which would lead to more plasticity in the fibres. However, trilobal fibres maintain the same mechanical properties as round fibres. IR thermography during liquid application of the same tampons three times consecutively, reveals a difference between the first measurement and additional measurements. This could be an indicator for energy stored in the tampon during production (form-pressing), that is released during expansion. However, the differences observed between tampons with mediocre and high absorbency

were only marginal, and it was not possible to substantiate the theory. The overall higher temperature of trilobal fibre tampons during liquid application could be due to the higher number of absorption sites, as identified in the SSA measurements. The geometry of trilobal fibres provides better tampon absorbency compared to standard viscose fibres, despite both types of fibres having similar mechanical properties at varying relative humidity levels, including when wet. While trilobal fibres exhibit higher swelling due to their higher fibre porosity, this alone does not fully explain their superior absorption performance. This could be due to the higher pore volume provided by trilobal fibres, as compared to tightly-packed round fibres. Hence, the absorbency of tampons is mostly determined by the network structure and is only slightly affected by fibre swelling.

Author contributions The manuscript was written through contributions of all authors. All authors have given approval to the final version of the manuscript.

Code availability Commercial software was used.

Declarations

Conflict of interest The authors declare that they have no known competing financial interests or personal relationships that could have appeared to influence the work reported in this paper.

References

Ahvenainen P, Kontro I, Svedström K (2016) Comparison of sample crystallinity determination methods by X-ray diffraction for challenging cellulose I materials. Cellulose 23:1073–1086. https://doi.org/10.1007/s10570-016-0881-6

Ajmeri JR, Ajmeri CJ (2010) Nonwoven personal hygiene materials and products. In: Applications of nonwovens in technical textiles. Elsevier, pp 85–102

Aslannejad H, Hassanizadeh SM (2017) Study of hydraulic properties of uncoated paper: image analysis and pore-scale modeling. Transp Porous Media 120:67–81. https://doi.org/10.1007/s11242-017-0909-x

Aslannejad H, Terzis A, Hassanizadeh SM, Weigand B (2017) Occurrence of temperature spikes at a wetting front during spontaneous imbibition. Sci Rep 7:1–15. https://doi.org/10.1038/s41598-017-07528-7

Bernt I (2011) Fine-tuning of paper characteristics by incorporation of viscose fibers. Lenzing Berichte 89:78–85

Cai J, Jin T, Kou J et al (2021) Lucas–Washburn equation-based modeling of capillary-driven flow in porous systems. Langmuir 37:1623–1636. https://doi.org/10.1021/acs.langmuir.0c03134

Conder JR, Young CL (1979) Physicochemical measurement by gas chromatography. Wiley, Hoboken

Dubrovski PD, Brezocnik M (2016) Porosity and nonwoven fabric vertical wicking rate. Fibers Polymers 17:801–808. https://doi.org/10.1007/s12221-016-6347-5

Fras Zemljic L, Sauperl O, But I et al (2011) Viscose material functionalized by chitosan as a potential treatment in gynecology. Textile Res J 81:1183–1190. https://doi.org/10.1177/0040517510397572

Ganser C, Kreiml P, Morak R et al (2015) The effects of water uptake on mechanical properties of viscose fibers. Cellulose 22:2777–2786. https://doi.org/10.1007/s10570-015-0666-3

Gellert DA (1984) U.S. Patent No. 4,475,911. U.S. Patent and Trademark Office, Washington, DC

Gupta BS (2002) Fluid absorption in high bulk nonwovens. In: Textile science and technology, vol 13. Elsevier, pp 93–127. https://doi.org/10.1016/S0920-4083(02)80006-8

Gupta BS (2008) Friction behavior of fibrous materials used in textiles. In: Friction in textile materials. Woodhead Publishing, pp 67–94. https://doi.org/10.1533/9781845694722.1.67

Hindeleh AM, Johnson DJ (1974) Crystallinity and crystallite size measurement in cellulose fibres: 2. Viscose Rayon. Polymer 15:697–705. https://doi.org/10.1016/0032-3861(74)90020-2

Horio M, Kobayashi K, Kondo T (1947) Investigation of fine structure of freely coagulated viscose fibers by means of optical and electron microscope. Text Res J 17:264–280. https://doi.org/10.1177/004051754701700503

Hou M, Acton PD (2016) Understanding the tampon density and density gradient through computed tomography imaging. Text Res J 86:573–579. https://doi.org/10.1177/0040517515595026

Hyll K (2016) Image-based quantitative infrared analysis and microparticle characterisation for pulp and paper applications. KTH Royal Institute of Technology, Stockholm

Kara S, Erdogan UH, Erdem N (2012) Effect of polypropylene fiber cross sectional shapes on some structural/mechanical fiber properties and compressibility behaviour of plain knitted fabrics. Fibers Polymers 13:790–794. https://doi.org/10.1007/s12221-012-0790-8

Kawase T, Sekoguchi S, Fujii T, Minagawa M (1986) Capillary spreading of liquids. Text Res J 56:409–414

Kissa E (1981) Capillary sorption in fibrous assemblies. J Colloid Interface Sci 83:265–272. https://doi.org/10.1016/0021-9797(81)90031-X

Kittelmann W (2004) Nonwovens for hygiene. Nonwoven fabrics. Wiley, Weinheim, pp 488–493

Klare H, Gröbe A (1962) Über die Wirkung des Zinksulfats in Spinnbädern bei der Fadenbildung von Celluloseregeneratfäden aus Viskose. Z Chem 2:15–19. https://doi.org/10.1002/zfch.19620020106

Krässig H (1993) Cellulose: structure, accessibility and reactivity. Gordon and Breach Science Publishers, Yverdon, Switzerland

Kreze T, Malej S (2003) Structural characteristics of new and conventional regenerated cellulosic fibers. Text Res J 73:675–684. https://doi.org/10.1177/004051750307300804

Lahti J, Dauer M, Keller DS, Hirn U (2020) Identifying the weak spots in packaging paper: local variations in grammage, fiber orientation and density and the resulting local strain and failure under load. Cellulose 27:10327–10343. https://doi.org/10.1007/s10570-020-03493-z

Lavi B, Marmur A (2006) The capillary race: optimal surface tensions for fastest penetration. Colloids Surf A Physicochem Eng Asp 282–283:263–271. https://doi.org/10.1016/j.colsurfa.2006.01.033

Leuk P, Schneeberger M, Hirn U, Bauer W (2016) Heat of sorption: a comparison between isotherm models and calorimeter measurements of wood pulp. Drying Technol 34:563–573. https://doi.org/10.1080/07373937.2015.1062391

Luan P, Zhao X, Copenhaver K et al (2022) Turning natural herbaceous fibers into advanced materials for sustainability. Adv Fiber Mater 4:736–757. https://doi.org/10.1007/s42765-022-00151-w

Lucas R (1918) Ueber das Zeitgesetz des kapillaren Aufstiegs von Flüssigkeiten. Kolloid Z 23:15–22. https://doi.org/10.1007/BF01461107

Ma J, Zhang N, Cheng Y et al (2022) Green fabrication of multifunctional three-dimensional superabsorbent nonwovens with thermo-bonding fibers. Adv Fiber Mater 4:293–304. https://doi.org/10.1007/s42765-021-00108-5

Mao N, Russell SJ, Pourdeyhimi B (2022) Characterisation, testing, and modelling of nonwoven fabrics. In: Handbook of nonwovens. Woodhead Publishing, pp 509–626. https://doi.org/10.1016/B978-0-12-818912-2.00008-2

Meirowitz RE, Riese JW, Phelan RJ (1994) U.S. Patent No. 5,314,743. U.S. Patent and Trademark Office, Washington, DC

Murali V, Zeegers JCH, Darhuber AA (2020) Infrared thermography of sorptive heating of thin porous media—experiments and continuum simulations. Int J Heat Mass Transf 147:118875. https://doi.org/10.1016/j.ijheatmasstransfer.2019.118875

Nachinkin OI (1973) The cross-sectional shape of man-made fibres. Fibre Chem 5:158–160. https://doi.org/10.1007/BF00546999

Nikonovich CV, Kerimova NG, Burchanova ND, Usmanov KhU (2007) The supermolecular structure of viscose fibers and its dependence on spinning conditions. J Polym Sci Polym Symp 42:1625–1637. https://doi.org/10.1002/polc.5070420365

Park S, Baker JO, Himmel ME et al (2010) Cellulose crystallinity index: measurement techniques and their impact on interpreting cellulase performance. Biotechnol Biofuels 3:1–10. https://doi.org/10.1186/1754-6834-3-10

Preston JM, Nimkar MV (1949) Measuring the swelling of fibres in water. J Textile Inst Proc 40:P674–P688. https://doi.org/10.1080/19447014908664692

Reame NK (2020) Toxic shock syndrome and tampons: the birth of a movement and a research 'Vagenda'. The Palgrave Handbook of Critical Menstruation Studies, pp 687–703. https://doi.org/10.1007/978-981-15-0614-7_51

Rees WH (1948) 30—The heat of absorption of water by cellulose. J Text Inst Trans 39:T351–T367. https://doi.org/10.1080/19447024808659435

Roggenstein W (2011) Viscose fibres with new functional qualities. Lenzing Berichte 89:72–77

Senden TJ, Bauer A, Roberts RJ, et al (2007) Experimental imaging of fluid penetration into papers. In: 61st Appita annual conference and exhibition, Gold Coast, Australia 6–9 May 2007: Proceedings May 2007. pp 149–153

Sierks MR, Reilly PJ (1985) Application of cross-linked carboxymethyl cellulose degradation by beta-glucosidase and vaginal microbes to toxic shock syndrome. Appl Environ Microbiol 50:634–637. https://doi.org/10.1128/aem.50.3.634-637.1985

Statista (2019) Forecast market value of tampons worldwide from 2018 to 2024 (in billion U.S. dollars) [Graph]. https://www.statista.com/statistics/920646/global-market-value-of-tampons/

Sun L, Chen JY, Jiang W, Lynch V (2015) Crystalline characteristics of cellulose fiber and film regenerated from ionic liquid solution. Carbohydr Polym 118:150–155. https://doi.org/10.1016/j.carbpol.2014.11.008

Vostral S (2017) Toxic shock syndrome, tampons and laboratory standard–setting. Can Med Assoc J 189:E726–E728. https://doi.org/10.1503/cmaj.161479

Waldner C, Hirn U (2023) Modeling liquid penetration into porous materials based on substrate and liquid surface energies. J Colloid Interface Sci 640:445–455. https://doi.org/10.1016/j.jcis.2023.02.116

Washburn EW (1921) The dynamics of capillary flow. Phys Rev 17:273–283. https://doi.org/10.1103/PhysRev.17.273

Whang HS, Gupta BS (2000) Surface wetting characteristics of cellulosic fibers. Text Res J 70:351–358. https://doi.org/10.1177/004051750007000412

Wilkes AG (2001) The viscose process. In: Regenerated cellulose fibres. Elsevier, pp 37–61

Wimmer P (2013) Viscose fibres for enhanced fluid management. Lenzing Berichte 91:61–66

Zambrano MC, Pawlak JJ, Daystar J et al (2019) Microfibers generated from the laundering of cotton, rayon and polyester based fabrics and their aquatic biodegradation. Mar Pollut Bull 142:394–407. https://doi.org/10.1016/j.marpolbul.2019.02.062